Published in final edited form as:
Lab Chip. 2011 December 21; 11(24): 4248–4259. doi:10.1039/c1lc20627c.

Dielectrophoretic Tweezers as a Platform for Molecular Force Spectroscopy in a Highly Parallel Format

Peng Cheng, **Michael J. Barrett**, **Piercen M. Oliver**, **Deniz Cetin**, and **Dmitri Vezenov***
Lehigh University, Department of Chemistry, 6 E. Packer Ave., Bethlehem, PA, 18015, USA

Abstract

We demonstrated the application of a simple electrode geometry for dielectrophoresis (DEP) on colloidal probes as a form of molecular force spectroscopy in a highly parallel format. The electric field between parallel plates is perturbed with dielectric microstructures, generating uniform DEP forces on colloidal probes in the range of several hundred piconewtons across a macroscopic sample area. We determined the approximate crossover frequency between negative and positive DEP using electrodes without dielectric microstructures—a simplification over standard experimental methods involving quadrupoles or optical trapping. 2D and 3D simulations of the electric field distributions validated the experimental behavior of several of our DEP tweezers geometries and provided insight into potential improvements. We applied the DEP tweezers to the stretching of a short DNA oligomer and detected its extension using total-internal reflection fluorescence microscopy. The combination of a simple cell fabrication, a uniform distribution of high axial forces, and a facile optical detection of our DEP tweezers makes this form of molecular force spectroscopy ideal for highly parallel detection of stretching or unbinding kinetics of biomolecules.

Introduction

In recent years, molecular force spectroscopy (MFS) has become a major research tool for studying inter- and intra-molecular forces, including biomolecular recognition,[1–4] the energy landscapes of protein folding,[5, 6] and energetic barriers of the conformational changes in biomolecules.[7, 8] A typical force spectroscopy experiment often involves binding one end of a molecule to a surface of a rigid support and the other to a mobile force probe (commonly a tip of an atomic force microscope (AFM) or a microsphere used in optical tweezers)[9, 10] followed by controlled displacement of the probe to obtain a force-extension curve.[11] In MFS experiments, hundreds of measurements must be collected on the same system in order to provide sufficient data for averaging and statistics or to uncover multiple unique mechanical pathways or states of the system. This experimental process is often time-consuming and cannot be readily extended to a parallel format, especially if chemically-distinct molecules are to be analyzed, since a different optical trap or AFM tip will be needed for multiple molecular species. Alternatively, magnetic tweezers provide an opportunity to acquire large amounts of data by simultaneously applying a magnetic field to multiple magnetic colloidal probes,[12–15] thereby applying a controlled force in parallel. However, the challenges in this case are the difficulty in fabrication of the monodisperse superparamagnetic probes, need for close proximity of the magnetic field concentrator to achieve high forces, and limited sample area where uniform force application can be achieved. Herein, we propose a massively parallel MFS technique based on dielectrophoresis (DEP), in which the force on the probes is evenly applied to all the probes in the system. We show that by perturbing the electric field with dielectric microstructures

dvezenov@lehigh.edu.

one can generate DEP forces in the range of several hundred piconewtons acting on microscopic probes across a macroscopic sample area. The magnitude and direction of the force can be manipulated by controlling the amplitude and frequency of the electric field.

In this paper, we report an implementation of dielectrophoretic tweezers using parallel flat electrodes to manipulate an array of polymer force probes. Instead of fabricating complex micro-electrode arrays to generate the field gradients necessary to manipulate particles with DEP (a common approach for applications of dielectrophoresis with biological samples),[16–23] we used a single set of macroscopic electrodes to generate high electric field gradients in the vicinity of the sample surface by using simple microfabricated dielectric structures (microwells) on one of the electrodes. Near a planar electrode, the force probe itself (a dielectric microsphere) can also serve as such a microstructure thereby creating the electric field gradient used to apply a force. We evaluated the performance characteristics of several possible designs for DEP tweezers using numerical analysis and then used this chip-based force spectroscopy technique to stretch single stranded DNA (ssDNA). Since we are using large area metal surfaces as electrodes, we can achieve a uniform potential distribution and reproducible field gradients throughout the whole working area of the device, thus, making this approach ideally suited for highly parallel measurements.

Theoretical background of DEP

The DEP phenomenon occurs when a dielectric material (in our case, a polymer microsphere) is exposed to a non-uniform electric field. The electric field polarizes both the dielectric particle and the medium around it to different extents and the material with the greater polarization (either the particle or the surrounding medium) will move towards the region of the higher electric field in order to lower the energy of interaction with the external electric field. To characterize the force acting on a probe in such a system, we can write the time averaged DEP force as:

$$\overline{F}=2\pi R^3 \varepsilon_m Re(CM)\nabla E_{rms}^2 \tag{1}$$

where R is the radius of the particle, ε_m is the dielectric constant of the medium, $Re(CM)$ is the real part of the Clausius-Mossotti (CM) factor,[24] and ∇E_{rms}^2 is the gradient of the squared electric field. The CM factor describes the total redistribution of charge throughout the system and takes into account the polarizabilities and the conductivities of both the particle and the medium.

$$CM(\tilde{\varepsilon}_p, \tilde{\varepsilon}_m)=\frac{\tilde{\varepsilon}_p-\tilde{\varepsilon}_m}{\tilde{\varepsilon}_p+2\tilde{\varepsilon}_m}, \tag{2}$$

where $\tilde{\varepsilon}_p$ and $\tilde{\varepsilon}_m$ are the complex dielectric constant of the particle and the medium, respectively. The complex dielectric constants depend on both the conductivity (σ) (of the polymer itself and the electric double layer[25–28]) and the relative permittivity (ε_r) of the material, as well as the frequency of the AC field (f) and is written as:

$$\tilde{\varepsilon}=\varepsilon_0\varepsilon_r-i\frac{\sigma}{2\pi f}. \tag{3}$$

An important aspect of the CM factor is that it introduces frequency dependence to the DEP force that one can potentially use to tune the magnitude of the DEP force or even reverse its direction. When $Re(CM)$ value is positive, the particle will move towards the high electric field, and the effect is termed positive DEP. In contrast, negative DEP occurs when the

value of the real part of the CM factor is negative, inducing the particle to move towards the low electric field. As a result, this physical relationship can be exploited to either push or pull on a polymer microsphere in an aqueous medium.

Figure 1 shows the calculated frequency dependence of the CM factor expected for the polymer-only microspheres used throughout this manuscript, in an ideal water environment assuming formation of an electric double layer. According to Equations 2 & 3, the frequency necessary to switch the DEP direction from positive to negative for colloidal probes in aqueous solutions lies around the 1 MHz range, which is easily obtainable with off-the-shelf function generators. This swappable force direction enables application of the proposed DEP tweezers in a wide range of different systems; for example, one can use the tweezers to trap and then release polymer particles or whole cells.

System Design

To produce a DEP force, one needs to form electric field gradient in the sample volume of interest. Commonly, closely positioned micropatterned electrodes are used to create a non-uniform electric field capable of generating a DEP force.[29–33] As an alternative to this method, it is possible to perturb the electric field with a dielectric structure (including the particle that one is trying to manipulate). [34–37]

A system of two parallel large area electrodes produces a uniform electric field and no DEP force is expected for a single microsphere suspended in the space between these electrodes. When the sphere is close to the surface of one of the electrodes (distance $\ll$ particle size), an imbalance of the field gradient is created on the two sides of the probe (facing the solution and facing the electrode), generating a net DEP force normal to the substrate. When the sphere moves further away from the electrode's surface (on the order of the probe radius) the classical picture emerges and the DEP force disappears. This phenomenon is ideally suited for use of large (micron size) probes to pull on molecules having contour lengths on the order of hundreds of nanometers attached to flat surfaces, since the probe will always remain close to the surface compared to its size. An assembly of microspheres on a planar electrode due to DEP forces has been previously investigated,[38–41] although only lateral inter-particle forces were of interest in this case.

Flat electrodes as described above are not always ideal to conduct parallel force spectroscopy experiments, because (i) they do not provide for the optimization of the magnitude of the forces and (ii) they create a random array of probes that lack the organization to process data on a very large scale. To maximize control over the DEP forces, as well as introduce order to the array, we can consider the creation of a patterned electrode array and the perturbation of the electric field with a dielectric structure integrated into the large area electrode. Creating patterned electrode arrays may involve sophisticated fabrication methods and raises possible alignment issues (e.g. position of the probe with respect to electrode will affect the magnitude of the force), thus increasing the cost and degree of difficulty needed to fabricate and operate a cell for DEP tweezers working on a large scale. Alternatively, to perturb the electric field, a dielectric obstacle can be placed inside the otherwise uniform field, [42, 43] such as a microfabricated solid structure, for example, a microwell array. For these reasons, we chose to focus solely on the design of dielectric patterns to form the electric field gradient. Figure 2 diagrams four such electrode configurations all capable of delivering DEP force. We have conducted theoretical simulations and experiments to characterize the DEP forces for all four configurations of the electrodes.

There are several advantages to the use of the microwell format shown in Figure 2b–d. First, when the probe is positioned inside a well, there are several interfaces where dielectric

constant experiences a significant jump. When potential is applied between two planar gold electrodes, the electric field will be strongly perturbed by the dielectric contrast of three different materials (the probe, the medium, and the microwell), resulting in a high electric field gradient inside the well. Second, this approach to generation of the DEP force only relies on conventional fabrication of the microwell arrays by a single step contact photolithography. Third, the wells will also provide a high degree of order for arrangement of the probes on the surface of the DEP cell to simplify indexing of the array and subsequent analysis. Finally, placement of the microspheres inside individual wells results in the added stability of the setup during fluid exchanges, which may be necessary to conduct biochemical reactions/binding without removing the probes. The shear force on a single force probe is minimized during exchange (flow) of the solution above the surface of the microwell array.

In order to create a system for molecular force spectroscopy that can accommodate a large number of individual experiments and applies an adjustable DEP force to each molecule at the same time, we mounted a DEP chip inside a fluid cell that is accessible for optical observations and enables controlled dosing of microscopic force probes and reagents. Wide field optical microscopy ensures simultaneous observations of multiple probes. Integration with microfluidics minimizes the volume of reagents used, so that the total cost of conducting single molecule pulling experiments is greatly reduced, which is important if the DEP tweezers are to be used in a bioanalysis assay.

Numerical and Experimental Methods

Numerical simulation

To investigate the magnitude of the DEP force in each variation of the DEP tweezers arrays, we used a finite element method software package (COMSOL Multiphysics, Burlington, MA). Due to the constraints of the size and complexity of the problem, and demands on computational time for the simulations of the electric field in the space around the probe and electrodes, the majority of our simulations were conducted as two dimensional (2D) approximations. In order to examine the accuracy of 2D simulation, we compared results from four types of simulations: 2D, reduced 3D (2D with axial symmetry), and full 3D with a round or square well (see supporting information (SI), section S1). In both 2D and 3D simulations, we solved a variant of Poisson's equation for potential distribution:

$$-\nabla \cdot (\varepsilon_0 \nabla V - \boldsymbol{P}) = \rho \tag{4}$$

in the electrostatics module. Here V is the electric potential, $\boldsymbol{P}$ is the electric polarization vector, and the ρ is the electric charge density.

A standard simulation consisted of two 44.2 μm wide electrodes separated by 20 μm (unless specified otherwise) of deionized water. On the lower electrode 4.2 μm wide dielectric wells (consisting of SU-8) were simulated with depths of 2, 4, 6, and 8 μm with rounded corners (0.2 μm curvature) to reduce sharp edge effects not present in experiment. To represent the format of an array, the left and right boundaries of the cell were set to a periodic condition to repeat the structure infinitely. To simulate the force on a probe a PMMA sphere was place inside the well just above the surface of the electrode. For the entire system physical values for the relative dielectric constants were used. A quasi-static potential field was simulated from the Laplace equation $\nabla^2 V = 0$ (V is the voltage) for surface potentials of +5 and −5 V. The 3D calculations share the same parameters with the 2D simulation. Both a square shaped well and a round shaped well were modeled in 3D.

We investigated the accuracy of two different integration methods for derivation of a DEP force (see section S1 in SI for details). Besides using the first order approximation -- effective dipole moment (EDA) model, which results in Equation 1, we also used a rigorous model and obtained the force by integration of the Maxwell stress tensor (MST) over the surface of the probe.[44] The general form for the time-averaged net DEP force resulting from the MST method is:

$$F_{DEP} = \frac{1}{4} Re(\tilde{\varepsilon}_m) \oint_A ((\vec{E}\vec{E}^* + \vec{E}^*\vec{E}) - |E|^2 \boldsymbol{U}) \cdot \vec{n}\, dA \quad (5)$$

where A is the surface area of the probe, $\vec{E}$ is the electric field outside the probe and $\boldsymbol{U}$ is the unit tensor. Both methods showed convergence to constant force values for mesh sizes below 25 nm. After we integrated the MST over the surface, we multiplied the resulting force by the maximum real part of the CM factor, which is equal to 1 for positive DEP and 0.5 for negative DEP. We found that the MST method produced very similar results for all models; forces for full 3D round and square well models agreed within 3–8 %, whereas reduced 3D or 2D models were different from the full 3D results by 15–20 % of the total force (with a potential varied between 1 and 10 V and electrode separations varied between 20 and 100 μm). In contrast, the EDA method, which assumes a slowly varying electric field (compared to the probe size), overestimated the forces by a factor of 1.8 (reduced 3D) or 5 (full 3D) with respect to the MST results. Since the results between the full and reduced 3D methods showed adequate agreement in the magnitude of forces, we used the reduced 3D method in all simulations unless otherwise noted.

Fabrication of the DEP chip

The general strategy of fabricating an array of wells on a cover glass is shown in SI, Fig. S3. A round (40 mm diameter) cover glass (Warner Instruments, MA) was cleaned in Piranha solution (a 3:2 mixture of 98 % H_2SO_4: 30 % H_2O_2) for 40 minutes. The cover glass was rinsed with deionized (DI) water and blown dry with filtered nitrogen. Titanium (4.5 nm) and gold (11 nm) films were deposited on the glass surface using an e-beam evaporator (Eddy Co. SYS-24, SC-20-Digital System Controller). The gold-coated cover glass was then cleaned by air plasma (Harrick Plasma, Ithaca, NY) on a high power setting for 1 min. SU-8 3005 resist (Microchem Co., MA), was used to construct wells of desired depth and size on the gold-coated cover glass following the procedure recommended by the manufacturer. The SEM image in Figure S4 shows the final microwell pattern having straight sidewalls and a flat bottom. The cell compatible with TIRF observations required two extra fabrication steps. In order to block the light from propagating in the SU-8 and interacting with the probe, a 130 nm gold film was first deposited instead of the 11 nm gold layer (using the e-beam evaporator). We calculated that the transmission of light through 130 nm gold layer is less than 0.1%. After exposure and development of the SU-8 pattern, the thick gold layer at the bottom of the well was etched using a standard gold etchant (4 g KI, 1 g I_2, and 80 mL DI-H_2O), as confirmed by transmission microscopy (SI, Figure S4). A final thin transparent gold film (4 nm titanium and 15 nm gold using an e-beam evaporator) was deposited, coating primarily the bottom of the well and the top of the SU8 resist, for use with the thiol-on-gold immobilization chemistry. The initial gold layer under the SU8 will block the light from reaching any probe that may reside on the surface of the resist.

Probe fabrication and activation

The fluorescent microspheres were synthesized by micro-emulsification of PMMA solutions that contained 1-oxazine (SI, Figure S6). The probes were washed three times with 1 mL of 100 mM MES (2-(*N*-morpholino)ethanesulfonic acid, MP Biomedicals) pH 5.4 buffer, centrifuged, and resuspended in the same buffer in a 1.5 mL centrifuge tube. For attachment

to ssDNA molecules, the probes were activated for 15 min by adding 10 mg of 1-ethyl-3-(3-dimethylaminopropyl)carbodiimide (EDC) and 10 mg of *N*-hydroxysulfosuccinimide (sulfo-NHS) to suspension. The probes were washed three times with 1 mL pH 8.0 phosphate buffer containing 0.1% TWEEN 20 (Calbiochem) before they were flushed into the cell.

End-modification of DNA

Our ssDNA oligomer was 142 base pairs long (82 nm) and produced in-house using standard ligation techniques. The model DNA contained 5′-amine and 3′-thiol end modifications (5′-NH_2-$(CH_2)_6$- TG TAG AGA CGT CGA CAG CTC ACA CTC GCA TAC GAG ACT ATA GTA CGT ATC GAT ACG TCA TCT GAT CAC GCA CGC ATA TGT AGA GCT AGT GAG CAC GTC GAT ATG ACA TGA TAG CAG TCG CTA GGT CAG ATC GTT CGA CTA GG -$(CH_2)_3$-S-S-CH_2CH_2OH-3′). The sequence was constructed in order to eliminate as much secondary structure as possible by randomly generating sequences with certain limitations. Namely, no repeats of any particular base more than three times in a row were allowed.

To create a 142mer ssDNA terminated with an amine on the 5′ end and a thiol group on the 3′ end, a 5′-amine terminated 71mer, a 3′-thiol terminated 71mer, and a 30mer complementary to 15 bases at non-modified ends of each 71mer (purchased from Integrated DNA Technologies) were annealed, and the 71mers were then ligated together. First, 4.5 μL of 1 mM aqueous solutions of each DNA oligo were mixed with 10 μL of an annealing buffer (100 mM Tris HCL, 1M NaCl, 10 mM EDTA) and diluted to 100 μL with autoclaved DI water. The solution was denatured by undergoing a heat cycle of 2 min at 95° C in a thermocycler (Techne TC-3000) followed by five cycles of 95° C for 15 s, 40° C for 15s, and 72° C for 60 s. At the end of the last cycle the system was annealed for 5 min at 72° C. This procedure resulted in 45 μM of DNA in a 100 μL solution. For ligation, 50 μL of the DNA solution were combined with 14 μL of 10x T4 ligase buffer and 18.75 μL of T4 DNA ligase (7500 units) (New England Biosciences), diluted to 150 μL with autoclaved DI water, and kept at 16 °C for 16 hours in the thermocycler. The product of ligation was separated from reaction mixture using a MinElute column (Qiagen) and eluted with 10 μL DI water. The DNA was purified from the 30mer and other side-products by a 6x TBE Urea gel (Invitrogen). After excising the band, the sample was eluted with 1x TBE buffer at 37 °C overnight. The final product was purified with a MinElute column and eluted with 20 μL of DI water. The final DNA concentration was 50 ng/μL (~1 μM).[45]

Substrate Preparation

The microwells were cleaned with air plasma for 1 minute, then placed in an ethanol bath for 10 min on a shaker table and finally dried with nitrogen. A self-assembled monolayer was formed by reacting a 1 mM aqueous solution of (11-mercaptoundecyl)tetra(ethylene glycol) (MutEG) with the Au substrate for 1 hour followed by a thorough DI water rinse. For single molecule stretching experiments with ssDNA, 1 μL of 1.5 μM solution of 142mer ssDNA was first unprotected by adding 4 μL of 5 mM *tris*(2-carboxyethyl)phosphine in 6× SSC buffer and incubating for 30 min. A competitive binding was then used to attach the DNA at a low density by placing 10 μL (5 μL of each) of 1:100 or 1:150 142mer ssDNA (mixture from previous step): MutEG (dissolved in 1 M NaCl PBS) mixture on the substrate for 2 hours. The DI water rinsed and nitrogen dried substrate was then incubated in 1mM MutEG solution for another hour.

DEP cell assembly and microscope setup

The substrates were installed on the bottom side of a commercially available fluid cell (RC30, Warner Instruments) and a plasma cleaned flat gold substrate is installed on the top plate and sealed with vacuum grease (Figure 3a). A 30 mm long copper foil tape (32 μm

thickness) was attached to the surface of each electrode. The top-plate and the bottom-plate were sealed together with a silicone gasket leaving a 100 μm gap. The two electrodes were then connected to a function generator (Model 645-G, BNC Co., CA). The cell was set onto a stage of the through-objective TIRF microscope (Olympus IX 71, equipped with 638 nm fiber optic coupled diode laser, (Coherent), Figure 3b). An excess of probes were added to the cell using an inlet port. The probes were then allowed to settle via gravity and those that did not occupy the wells were washed away. A fluorescent microscopy image (Figure 3c) showed more than 80% occupancy of the micro-wells after the probes were infused into the assembled fluid cell.

For non-specific binding experiments, the probes were suspended in 0.1% solution of TWEEN 20 in DI water or phosphate buffer (pH 7.4) at 1 or 10 mM total ionic strength and flushed into the microfluidic cell. For the frequency scan experiment on a flat substrate, the probes settled down close to the surface by gravity. A frequency sweep with different scan rates under a constant potential was applied to the two electrodes while a video was captured by a CCD camera (Andor Technologies, iXon DV888, Belfast, Ireland). The number of probes and the integrated intensity of individual probes were calculated from analysis of the videos using custom code written in Igor Pro 6.2 (WaveMetrics, OR). Initial probe locations were found by thresholding the image and then (more accurately) from a fit to a 2-D Gaussian function. For each probe, a circular region of interest (ROI) was set around the center of the probe at a diameter of 10 μm (approximately five times the FWHM of the probe intensity profile). For each ROI, the background was first subtracted using a plane fit to a 1 μm-wide band surrounding the ROI. Probe intensities were then computed by numerical integration over the ROI. For ssDNA single molecule stretching experiment, the NHS-activated probes were flushed into the cell and settled down in the wells by gravity. The probes were incubated for 10 min inside the wells in order to attach to the ssDNA molecules (Figure 3b). A sinusoidal potential modulation was applied to the two electrodes to stretch the DNA while a video was recorded.

Results and Discussion

Molecular force spectroscopy provides information about a molecule's intra- and intermolecular forces through the measurement of force-distance profiles. The simulations and experiments described in this paper sought to determine the applicability of our DEP setup as a standalone force spectroscopy technique for parallel measurement. Three common aspects of force spectroscopy are usually considered: (i) a high force magnitude (> 1nN) in a controllable direction (compression or extension), (ii) high force resolution (~1 pN), and (iii) sensitive detection of molecular extension (<1 nm). We addressed each of these aspects with respect to critical factors such as applied voltage, electrode separation, frequency of applied field, probe position, and microwell geometry.

Voltage dependence of DEP force

One can vary the DEP force exerted on the probe by adjusting potential difference between the two electrodes ($F_{DEP} \sim V^2$, Equation 1). We computed the DEP force for flat electrodes (Geometry A) through the MST integration by sweeping peak-to-peak voltage from 0 V to 10 V for the planar electrode cell (SI, Figure S7). The results of the numerical analysis indicated an excellent agreement with the formal voltage dependence (a power law exponent of exactly 2) expected from the approximate model (Equation 1). Therefore, modulation of the DEP force can be readily achieved via the electrode potential. Using this method the force resolution would be defined by the resolution and stability of the driving electronics (according to Equation 1, for the simulated design, the relative noise in applied force should stay constant throughout voltage sweep, $\delta F/F = 2\delta V/V$, and 1 mV RMS noise will correspond to a 0.2 pN resolution at 10 V and 10 fN at 1 V). Since the shape of the field

gradient is set by the geometry of the setup and the local field scales with voltage, this voltage dependence of the DEP force holds for all other chip designs, as we confirmed by simulations of the DEP force on probes placed in 4 μm deep microwells (see SI, Figure S7).

Effect of the spacing between two electrodes

At a fixed potential difference, the magnitude of the electric field, E, in the space confined by the large area electrodes depends on their separation, s (for parallel electrodes in Geometry A, $E \propto 1/s$ and $F_{DEP} \propto E\nabla E \propto 1/s^2$). We found that the magnitude of the DEP force quickly decays with increasing distance between the two electrodes for both flat substrates and microwell designs. According to our simulations, for a 20 μm separation between electrodes, the DEP force of several hundred piconewton is readily achieved with both flat and micropatterned electrode configurations. For flat electrodes (Geometry A), the applied force dropped by two orders of magnitude, from 450 pN to 4 pN, (Figure 4) when the separation between electrodes increases from 20 μm to 200 μm. In contrast, when we placed a 3 μm diameter probe inside a 4 μm deep microwell (Geometry C, Figure 2c), the calculated force decreased gradually from 980 pN to 80 pN when electrodes moved apart from 20 μm to 200 μm.

By fitting the DEP force decay for flat electrodes to a power law (Figure 4), we determined that $1/s^2$ relationship fits this decay precisely, implying that for large electrode separations ($s \ll R$) the distribution of the electric field in this geometry does not change with the electrode gap (i.e. $E(z, s) \approx V/s\, f(z)$, where function f(z) characterizes electric field distribution for all s). For the microwells, the fit unexpectedly deviates from the $F_{DEP} \propto 1/s^2$ form (we obtained a best-fit exponent of 0.600 ± 0.033). We inspected numerical values of the electric field in the system and determined that this deviation is a result of our two layer arrangement (SU-8 and water). Since we are effectively using two parallel dielectrics in our system, the relative contributions (to the overall voltage between electrodes) of potential drops across each layer change with gap size causing a deviation from the expected power law. This effect is not present in a one-layer system. The electric field in the SU8 layer in this capacitor is:

$$E_{resist} = \frac{V}{s\frac{\varepsilon_{resist}}{\varepsilon_m} + h\left(1 + \frac{\varepsilon_{resist}}{\varepsilon_m}\right)} \tag{6}$$

where ε_{resist} is the dielectric constant of photoresist and ε_m is the dielectric constant of medium. By fitting the decay in the graph to the square of this function we see that the observed decrease in the DEP force follows a decay law related to the magnitude of the electric field in the resist.

The results from Figure 4 demonstrate that the DEP tweezers have a limitation on the maximum achievable force, requiring close proximity between the electrodes to attain a measurable DEP force. Although the force generated with a 20 μm gap for both flat and patterned electrodes is sufficient for most applications in force spectroscopy, the fabrication, handling, and storing components of such a device will pose some challenges. For example, it is hard to fabricate and handle a 20 μm thick elastomeric gasket to seal the DEP cell for fluid delivery. Therefore, to ensure an adequate range of forces (~100 pN) for Geometry A, the seal must be fabricated into one of the electrodes. On the other hand, the microwell geometry is not as sensitive to electrode separation and gaskets as thick as 100–200 μm appear suitable for a DEP cell, simplifying assembly of the microfluidic cell. For example, we successfully used a commercial fluid cell that places a polymer gasket between top-plate and bottom-plate to seal the system.

Frequency dependence of the DEP forces

Within any one of the DEP tweezers geometries, the microspheres can be pulled away from the surface or pushed towards the surface by switching between positive and negative DEP. Both regimes are readily achievable by operating at an appropriate frequency of the AC field (Figure 1). Since the CM factor is a property of the probe and the medium only, we used the simplest electrode setup of two parallel plates to determine the crossover frequency. Using flat electrodes (Geometry A), dispersed probes were allowed to settle onto the surface of the bottom electrode via gravity and then (i) either a stepped potential (0 to 10V) was applied to the cell at a fixed frequency or (ii) the potential was held constant (V_{pp}=10 V) while modulating the frequency from 1 MHz to 1 kHz. Using TIRF detection, with a 70° angle of incidence, we captured movies of the probes present near sample surface (probes lifted from the surface by the DEP force into bulk solution do not fluoresce due to TIR illumination conditions).

Without an applied voltage, the probe population remained suspended some distance (up to 200 nm) above the surface trapped in a potential well formed by the repulsive double layer forces and attraction due to gravity. In this state, the thermally activated movement of the probes in the soft potential well resulted in significant fluctuations in intensity (comparable to their mean intensity). When the high frequency (>100 kHz) field was applied, the probe fluorescence became more intense (Figure 5 - right inset) and fluctuations in intensity were reduced, indicating that the DEP force drove the probes toward the surface. Conversely, when the field was applied at a low frequency (<10 kHz), the intensity of the fluorescence dropped to zero, indicating the probes were driven off the surface completely (Figure 5 - left inset). Thus, positive DEP moves the polymer beads away from the flat electrode, whereas negative DEP attracts them to the surface.

In order to acquire the full frequency response of the probes in our system, we continuously monitored the number of probes in the vicinity of the surface (using TIRF) over the course of a frequency sweep at three different ionic strengths. The results shown in Figure 5 represent the changes of the CM factor with frequency of the AC field in our system. The crossover between positive and negative DEP occurs at between 50 and 100 kHz and depends on the bead's surface (electrical double layer) conductivity, which changes with the ionic strength of the buffer. The method we describe here was highly reproducible (2–3% error for crossover frequency obtained in repeated experiments), independent of the rate of frequency sweep (between 1 and 4 decades per minute). Unlike the use of quadrupole electrodes,[27] optical trapping[28] or patterned electrodes,[46] our method is very straightforward to implement under different solution conditions for beads of various compositions and properties. Any proposed design of DEP tweezers can be quickly evaluated for the frequency dependence of the directionality of the force by carrying out a frequency sweep experiment with probes having inert chemistry (to ensure that they contact the surface of the electrode in a fully reversible manner). For example, we determined experimentally that microwells having a depth greater than the bead diameter (Geometry C) result in repulsion from the surface under positive DEP conditions (low frequency), whereas microwells with depths smaller than bead diameter (Geometry B) display attractive forces under the same conditions.

Changes in the DEP force magnitude with position of the probe

With single molecule force spectroscopy, one could study specific binding events (i.e. breaking of intermolecular contacts) as well as conformational changes and stretching of biopolymers (DNA and proteins) that could require a force probe to move by as much as 100–1000 nm, depending on the contour length of the biomolecule. Since field inhomogeneity is produced by microscopic features, changes in the DEP force experienced

by probes moving near the surface of the electrode constitute an important characteristic in the design of the DEP tweezers.

Normal forces—When a dielectric probe is placed between the two planar electrodes, the probe itself induces inhomogeneity in the electric field. Numerical calculations show a difference in the density of electric field lines above and below the probe in contact with the electrode (Figure 6a). The overall electric field is higher at the top half of the probe than at the bottom, so that the probe will move away from the electrode under conditions of the positive DEP, as indeed observed in our experiments (Figure 5). When the probe is displaced away from the surface, the asymmetry is gradually lost as the electric field intensity above and below the probe becomes balanced (Figure 6b), resulting in no net DEP force as expected for a dielectric probe suspended in a uniform electric field. The DEP force drops down to one half of its maximum value within 1 μm from the surface.

Once the probes are placed inside the microwells, the contrast in the intensity of the electric field around the probes markedly increases (Figure 6c–f) leading to forces higher than for a probe near a non-structured interface. For shallow wells (Geometry B), the high field is concentrated near the edges of the well. As a result, at any distance from the surface, the parts of the probe facing the sample experience a higher field than the parts facing the solution. This situation is opposite to what we found for flat electrodes (Geometry A). The DEP cell with shallow microwells (Geometry B) will produce a repulsive force at negative DEP (high frequency). Indeed, a voltage step from 0 to 1 V at 1 MHz results in the removal of the 3 μm probes from 1 μm deep wells in our experiments.

When the depth of a microwell exceeds the size of the probe (Geometry C), the overall force profile represents a superposition of two opposing effects (i) a decrease of the electric field between the probe and electrode surface and (ii) an increase of the field around the edges of the well. For positive DEP (low frequency), the resulting force is repulsive and moves the bead away from the surface at small bead-electrode separations (<0.5 μm for a 4 μm deep well), whereas the force is attractive at large separations. For such a geometry, the probes can be trapped inside the well at some stable vertical position elevated above the surface, representing potential energy minimum for positive DEP (Figure 6i, l). Experiments with this design produced a stable trapping position for 3 μm diameter microspheres inside the microwells as demonstrated with far-field epi-fluorescence. (Figure 7). The probes inside the well moved out of the focus, but stayed inside the wells, when the frequency was changed from 100 kHz to 1 kHz. In contrast, the intensity profiles of the beads on top of the SU8 layer show perfect overlap at 100 kHz and 1 kHz as expected for stationary probes, since now realignment was done during frequency shift.

The competition between the two effects results in a quicker decay of the force with distance than for planar electrodes. The DEP force drops down to one half of its maximum value within 200–400 nm from the surface for 4–8 μm deep wells. On the other hand, the maximum force experienced by the probe in contact with the surface more than doubles compared to the flat electrode (Geometry A) due to the concentration of the field inside the microwell containing the buffer solution having a higher polarizability than the adjacent photoresist.

The change of the force with increase of the probe separation from the electrode is a potential drawback of the DEP tweezers, since, in addition to calibration with respect to applied voltage and probe size for a given microwell design, the forces need to be measured or calibrated at every position of the probe. This requirement, however, is not substantially different form the need to measure forces at every experimental point in the force-distance curves obtained using common force spectroscopy methods such as AFM or optical

tweezers. In principle, one can calibrate forces in DEP tweezers using thermal fluctuations in the probe position with either *x*-*y* or *z* tracking[47, 48] as is done for magnetic or optical tweezers. Since according in our simulations, the DEP force appears linear with respect to bead-surface separation at displacements below several hundred nanometers, one can also derive the DEP forces by calibrating this linear correlation; thus, only applied voltage and probe-surface distance will be required for the calculation of the DEP force experienced by the probe.[49]

Lateral forces—One can expect an imbalance of the electric field distribution, if the bead is not centered laterally in the microwell for Geometries B-D. A smaller gap between the probe and the wall results in a higher field intensity. This uneven electric field produces a lateral force that pulls the probes towards the wall during positive DEP and repels them from the wall under negative DEP conditions (Figure 8). Force spectroscopy operates by pulling the bead away from the surface, thereby stretching the attached molecule. In deep wells (Geometries C & D), a stretching force is applied using positive DEP, while shallow wells (Geometry B) use negative DEP.

Inspecting the relative magnitude of normal and later forces (Figure 8a), we observe that for deep wells it is crucial to have the probes properly centered, whereas some misalignment can be tolerated for shallow wells. Nevertheless, use of the deep wells may be preferred to shallow wells, because the required alignment can be achieved in the course of the attachment step by application of the negative DEP to trap the bead in the microwell (negative DEP traps and centers the probe in this case,). The probe will be axially centered by lateral forces at negative DEP (see Figure 8b) and its position fixed by the molecule attached between the electrode and the probe. Alternatively, one can make the top surface of the pattern conductive as well (by the second metal coating step) as in the DEP cell with Geometry D (Figure 2d). This cell produces no noticeable lateral force (Figure 8a) and centering of the bead inside the well becomes unimportant.

Measurements of molecular extension

The *z*-position of a microsphere near surface could be found using analysis of images from reflectance interference microscopy[50] or TIRF microscopy.[47, 51, 52] Both methods are compatible with flat electrodes, however, for structured electrodes, TIRF microscopy is preferred because only total intensity of the probe fluorescence or scattering intensity is needed to map the vertical position of the probe.[53] We used through-objective laser TIRF in our experiments with DEP tweezers. To achieve TIR conditions at the bottom of the microwells, the incident laser beam must be prevented from entering the SU-8 resist layer, since otherwise propagating light conditions will be achieved effectively throughout the whole sample. A thick metal layer between the glass substrate and resist layer in the DEP cell design shown in Figure 2d (Geometry D) serves this purpose (see SI, Figure S5).

Stretching of single stranded DNA molecules using DEP tweezers

To demonstrate the ability of the proposed DEP tweezers to conduct single molecule force spectroscopy, we used a model system of ssDNA. We tethered the DEP probe to the surface via a 142 base long DNA oligomer using the reaction scheme depicted in Figure 9.[49] The synthetic sequence contained two different terminal functional groups (thiol and amine) to facilitate attachment chemistry to gold electrode and poly(methyl methacrylate) microspheres bearing surface carboxyl groups. After the beads were flushed into the fluid cell and tethered to ssDNA molecules attached to the bottom of the wells, about 80% of the wells were occupied with the force probes (Figure 10a).

After attachment of probes, we applied a 1 kHz AC field to electrodes in the DEP fluid cell (Geometry D, Figure 2d, see Figure S8 for force decay plot) and modulated the peak-to-peak voltage between 0 V and 10 V to stretch the DNA. When the AC field was applied, about 25% of the captured probes left the surface, indicating that these probes were not covalently bound to the ssDNA. The remaining probes showed intensity oscillations when we modulated the amplitude of AC voltage. At low forces (low voltage amplitude), the DNA is compact and probes are close to the surface of the electrode (i.e. the interface for TIR). As the voltage amplitude is ramped up, the probes move away from the surface, extending the DNA molecules. As expected for TIRF illumination, the fluorescence of the beads is brighter at low voltage than at high voltage (compare images in Figure 10b). The fluorescence intensities of the beads that move away from the surface at high voltage amplitude decay about 50% on average. According to the force-extension curve of ssDNA molecule, the estimated DEP force exerted on a probe is between 15 and 25 picoNewtons.[49]

The TIRF-illumination images of the probes in Figure 10a show a wide distribution of intensities. This variation can be attributed to a number of factors: (i) non-uniform particle size, (ii) differences in the lateral positions of probes in the wells, and (iii) a non-uniform (Gaussian) illuminating intensity distribution in the field of view. We have measured a moderate polydispersity of probes sizes (up to a factor of two difference in diameters) and, since the fluorescence intensity is proportional to the volume, this polydispersity can yield up to an order of magnitude difference in brightness. The probe position and the light distribution of the probe inside the well are related. Simulations show an uneven lateral distribution of light inside the wells (Figure S9), which decreases in intensity as the probes move closer to the edges. Finally, it may be possible that the thick gold layer on the bottom of the well is not fully etched for every well, thus blocking an unknown percentage of the illumination and emission of the probes.

We are able to record movies of active probes (those that exhibited a change in intensity upon application of force) and record multiple force-extension curves for an array of the DNA molecules. As can be seen from the time traces of the total fluorescence intensity shown in Figure 10c, the force-extension curves for individual molecules are very reproducible and one can acquire high-quality data from multiple molecules in parallel. In this particular frame, 27 force probes populated 50 microwells and most of them showed the behaviour expected for single molecule stretching (only a few produced changes in intensity consistent with multi-tether attachment). The current DEP tweezers setup can already be used in qualitative analysis, for example, in the case of the ssDNA used here, to detect binding of the DNA-binding proteins or hybridization with a complementary oligomer. Quantitative force spectroscopy will require proper calibration of forces and bead-surface distances as well as the light intensity field in the microwells, all of which are the focus of our on-going work with this system.

Conclusions

We proposed a new single molecule force spectroscopy method based on dielectrophoresis —DEP tweezers. Numerical simulations suggest that forces on the order of 1 nN can be readily achieved with a 10 V peak-to-peak AC voltage applied to a DEP cell. The direction of the force can be switched by selecting the frequency regime appropriate for either positive or negative DEP. The parallel-plate electrodes DEP cell design can serve as a simple device to map the crossover frequency between the two DEP regimes for different probes and solution conditions without setting up the quadruple electrodes or integrating the DEP device with the optical tweezers.

There are several disadvantages to this method of manipulation of the force probes: (i) DEP forces acting on a colloidal probe decay quickly with its distance from the electrode (within 200–500 nm); (ii) the maximum force achieved in the DEP tweezers drops rapidly (inversely quadratic) with an increase in the inter-electrode gap; and (iii) forces need to be measured or calibrated independently for each position of the probe. Some of these difficulties can be alleviated by using microstructured electrodes; for example, microwells can increase the maximum force on the beads and greatly reduce the dependence of the DEP force on the inter-electrode spacing. Microwell arrays can have added benefits for DEP tweezers by increasing the density of the probes on the surface, simplifying bead indexing, and improving stability of the probe-molecule assembly by reducing shear forces during exchange of the solution inside the fluid cell. The final assembled instrument was applied to stretching of the ssDNA molecules and demonstrated reproducible operation in stretching single DNA molecules.

We have examined a variety of chip geometries for highly parallel force spectroscopy, each with its own set of advantages and limitations. We feel that, with the selection of geometries described in this paper, most applications involving some form of force application should be amenable to DEP tweezers. For applications where the applied force must be known quantitatively (such as in protein unfolding or DNA stretching) a middle ground must be reached between the magnitude of the forces and complexity of the cell design and data analysis. One has to compromise between small variations in the magnitude of the forces (less than an order of magnitude) due to positioning and size, and the need for an individual calibration of the forces on each probe in order to measure the forces in an arbitrary system. Refinement of the uniformity of the experimental implementation of the DEP tweezers (e.g. use of symmetrical round wells and monodisperse probes) can also alleviate the issues of device calibration. As opposed to the microwell geometry, the planar electrode produces more uniform forces across the entire working area making it easier to directly compare the results of adjacent probes at the expense of reduced force magnitude and the need for slower fluid exchange. If both conditions are required (high forces and a calibrated force magnitude) one can use the microwell geometry with a force calibration based on the Brownian diffusion of the probes under applied force.[54, 55]

Supplementary Material

Refer to Web version on PubMed Central for supplementary material.

Acknowledgments

We acknowledge funding of this work by NIH grant R21 HG004141. We used instruments supported by NSF Major Research Instrumentation grant CHE-0923370.

References

1. Willemsen OH, Snel MME, Cambi A, Greve J, De Grooth BG, Figdor CG. Biophysical Journal. 2000; 79:3267–3281. [PubMed: 11106630]
2. Janshoff A, Neitzert M, Oberdorfer Y, Fuchs H. Angewandte Chemie. 2000; 39:3212–3237. [PubMed: 11028062]
3. Vezenov DV, Noy A, Rozsnyai LF, Lieber CM. Journal of the American Chemical Society. 1997; 119:2006–2015.
4. Noy A. Surface and Interface Analysis. 2006; 38:1429–1441.
5. Rief M, Pascual J, Saraste M, Gaub HE. Journal of Molecular Biology. 1999; 286:553–561. [PubMed: 9973570]
6. Barsegov V, Klimov DK, Thirumalai D. Biophysical Journal. 2006; 90:3827–3841. [PubMed: 16533852]

7. Rief M, Grubmüller H. Chem Phys Chem. 2002; 3:255–261. [PubMed: 12503171]
8. Thirumalai D, O'Brien EP, Morrison G, Hyeon C. Annual Review of Biophysics. 2010; 39:159–183.
9. Neuman KC, Nagy A. Nat Meth. 2008; 5:491–505.
10. Noy A, Vezenov DV, Lieber CM. Handbook of Molecular Force Spectroscopy. 2008:97–122.
11. Liang J, Fernandez JM. ACS Nano. 2009; 3:1628–1645. [PubMed: 19572737]
12. Conroy, R. Handbook of Molecular Force Spectroscopy. Noy, A., editor. Vol. 2. Springer; New York, NY: 2008. p. 23-96.
13. Kruithof M, Chien F, De Jager M, Van Noort J. Biophysical Journal. 2008; 94:2343–2348. [PubMed: 18065448]
14. Gosse C, Croquette V. Biophysical Journal. 2002; 82:3314–3329. [PubMed: 12023254]
15. Yang Y, Erb RM, Wiley BJ, Zauscher S, Yellen BB. Nano Letters. 2011; 11:1681–1684. [PubMed: 21417363]
16. Baek SH, Chang W-J, Baek J-Y, Yoon DS, Bashir R, Lee SW. Analytical Chemistry. 2009; 81:7737–7742. [PubMed: 19663393]
17. Voldman J. Annual Review of Biomedical Engineering. 2006; 8:425–454.
18. Cheng IF, Froude VE, Zhu Y, Chang H-C, Chang H-C. Lab on a Chip. 2009; 9:3193–3201. [PubMed: 19865725]
19. Cui H-H, Voldman J, He X-F, Lim K-M. Lab on a Chip. 2009; 9:2306–2312. [PubMed: 19636460]
20. Fan S-K, Hsieh T-H, Lin D-Y. Lab on a Chip. 2009; 9:1236–1242. [PubMed: 19370242]
21. Gagnon Z, Mazur J, Chang H-C. Lab on a Chip. 2009; 10:718–726. [PubMed: 20221559]
22. Kuo C-T, Liu C-H. Lab on a Chip. 2008; 8:725–733. [PubMed: 18432342]
23. Squires TM. Lab on a Chip. 2009; 9:2477–2483. [PubMed: 19680573]
24. Jones TB. Engineering in Medicine and Biology Magazine, IEEE. 2003; 22:33–42.
25. Curtis HJ, Fricke H. Physical Review. 1935; 48:775.
26. Green NG, Morgan H. Journal of Physics D: Applied Physics. 1997; 30:2626.
27. Green NG, Morgan H. The Journal of Physical Chemistry B. 1998; 103:41–50.
28. Wei M-T, Junio J, Ou-Yang HD. Biomicrofluidics. 2009; 3:012003–012008.
29. Hsiung L-C, Chiang C-L, Wang C-H, Huang Y-H, Kuo C-T, Cheng J-Y, Lin C-H, Wu V, Chou H-Y, Jong D-S, Lee H, Wo AM. Lab on a Chip. 2011; 11:2333–2342. [PubMed: 21629948]
30. Choi S, Park J-K. Lab on a Chip. 2005; 5:1161–1167. [PubMed: 16175274]
31. Shafiee H, Sano MB, Henslee EA, Caldwell JL, Davalos RV. Lab on a Chip. 2010; 10:438–445. [PubMed: 20126683]
32. Morgan H, Hughes MP, Green NG. Biophysical Journal. 1999; 77:516–525. [PubMed: 10388776]
33. Oh J, Hart R, Capurro J, Noh H. Lab on a Chip. 2009; 9:62–78. [PubMed: 19209337]
34. Barbee KD, Hsiao AP, Roller EE, Huang X. Lab on a Chip. 2010; 10:3084–3093. [PubMed: 20820631]
35. Qiao W, Cho G, Lo Y-H. Lab on a Chip. 2011; 11:1074–1080. [PubMed: 21293829]
36. Xu Y, Yao H, Wang L, Xing W, Cheng J. Lab on a Chip. 2011; 11:2417–2423. [PubMed: 21625729]
37. Krishnan M, Mojarad N, Kukura P, Sandoghdar V. Nature. 2010; 467:692–695. [PubMed: 20930840]
38. Ristenpart WD, Aksay IA, Saville DA. Physical Review Letters. 2003; 90:128303. [PubMed: 12688910]
39. Winkleman A, McCarty LS, Ting Z, Weibel DB, Zhigang S, Whitesides GM. Microelectromechanical Systems, Journal of. 2008; 17:900–910.
40. Prieve DC, Sides PJ, Wirth CL. Current Opinion in Colloid & Interface Science. 2010; 15:160–174.
41. Winkleman A, Gates BD, McCarty LS, Whitesides GM. Advanced Materials. 2005; 17:1507–1511.
42. Barbulovic-Nad I, Xuan X, Lee JSH, Li D. Lab on a Chip. 2006; 6:274–279. [PubMed: 16450038]

43. Chu H, Doh I, Cho Y-H. Lab on a Chip. 2009; 9:686–691. [PubMed: 19224018]
44. Wang X, Wang X-B, Gascoyne PRC. Journal of Electrostatics. 1997; 39:277–295.
45. Lim HI, Oliver PM, Marzillier J, Vezenov DV. Analytical and Bioanalytical Chemistry. 2010; 397:1861–1872. [PubMed: 20422158]
46. Juarez JJ, Cui J-Q, Liu BG, Bevan MA. Langmuir. 2011:null–null.
47. Prieve DC. Advances in Colloid and Interface Science. 1999; 82:93–125.
48. Bevan MA, Prieve DC. The Journal of Chemical Physics. 2000; 113:1228–1236.
49. Oliver PM, Park JS, Vezenov D. Nanoscale. 2011; 3:581–591. [PubMed: 21103547]
50. Verschueren H. Journal of Cell Science. 1985; 75:279–301. [PubMed: 3900106]
51. Wazawa T, Ueda M. Microscopy Techniques. 2005:77–106.
52. Hertlein C, Riefler N, Eremina E, Wriedt T, Eremin Y, Helden L, Bechinger C. Langmuir. 2008; 24:1–4. [PubMed: 18052301]
53. Bijamov A, Shubitidze F, Oliver PM, Vezenov DV. Langmuir. 2010; 26:12003–12011. [PubMed: 20486724]
54. Dennis CP. Advances in Colloid and Interface Science. 1999; 82:93–125.
55. Bevan M. J Chem Phys. 2000; 113:1228.

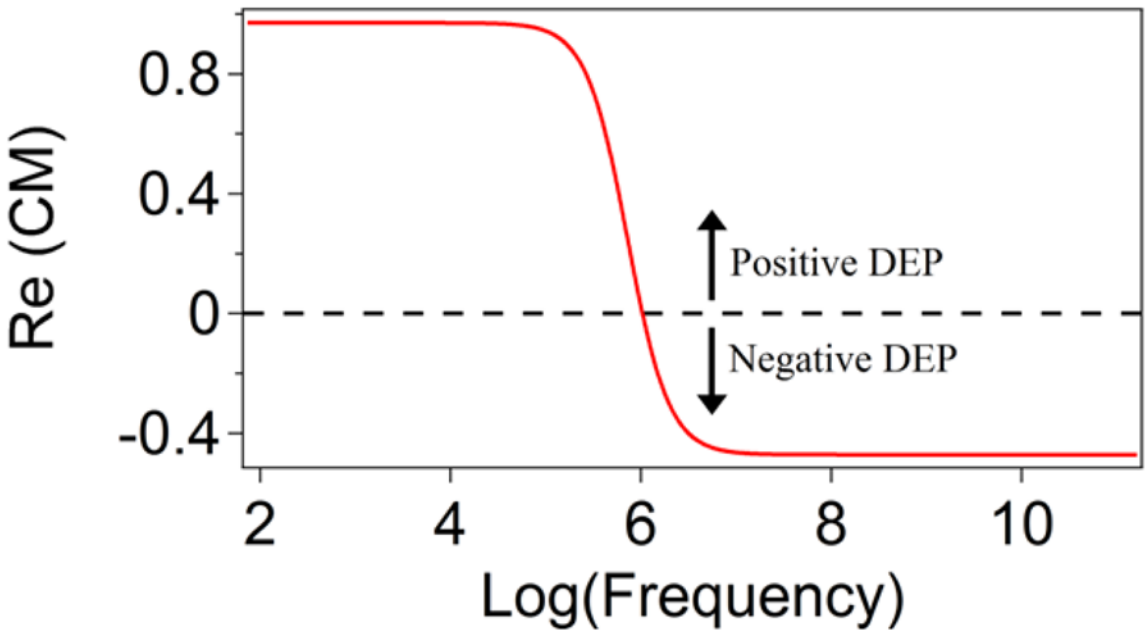

Figure 1.
Calculated frequency dependence of the real part of the Clausius-Mossotti factor for a dielectric particle typical to our system ($\varepsilon_m/\varepsilon_0 = 78$, $\sigma_m = 10^{-5}S \cdot m^{-1}$; $\varepsilon_p/\varepsilon_0 = 3.0$, $\sigma_p = 10^{-3}S \cdot m^{-1}$). The probe experiences a positive DEP force when the frequency is below 1 MHz, while a negative DEP force acts on a probe when the frequency of applied AC field is above 1 MHz.

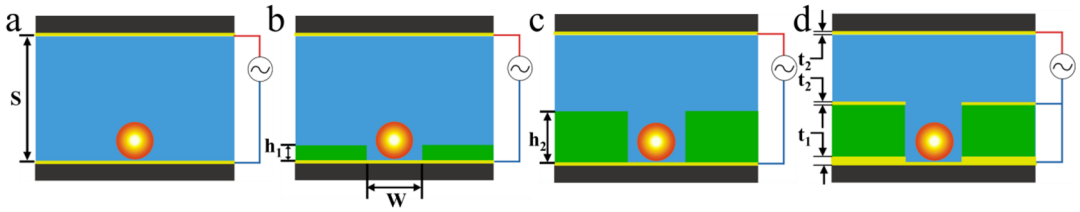

Figure 2.

Various cell designs for DEP tweezers. (a) Geometry A: A probe above a flat electrode. (b) Geometry B: A probe in a shallow microwell fabricated on top of an electrode (well depth h_1 < bead diameter). (c) Geometry C: A probe inside a deep microwell fabricated on top of an electrode (well depth h_2 > bead diameter). (d) Geometry D: A microwell on top of a thick gold layer (thickness t_1=135 nm), whose primary purpose is to block the light from entering the photoresist layer making layout suitable for TIRFM detection. The thin gold layers (thickness t_2=14 nm) act as the electrodes. The standard dimensions for all wells used in this work had w=4.2 μm and s=24 μm (unless varied on purpose). The center-to-center distance for the wells was 44.2 μm.

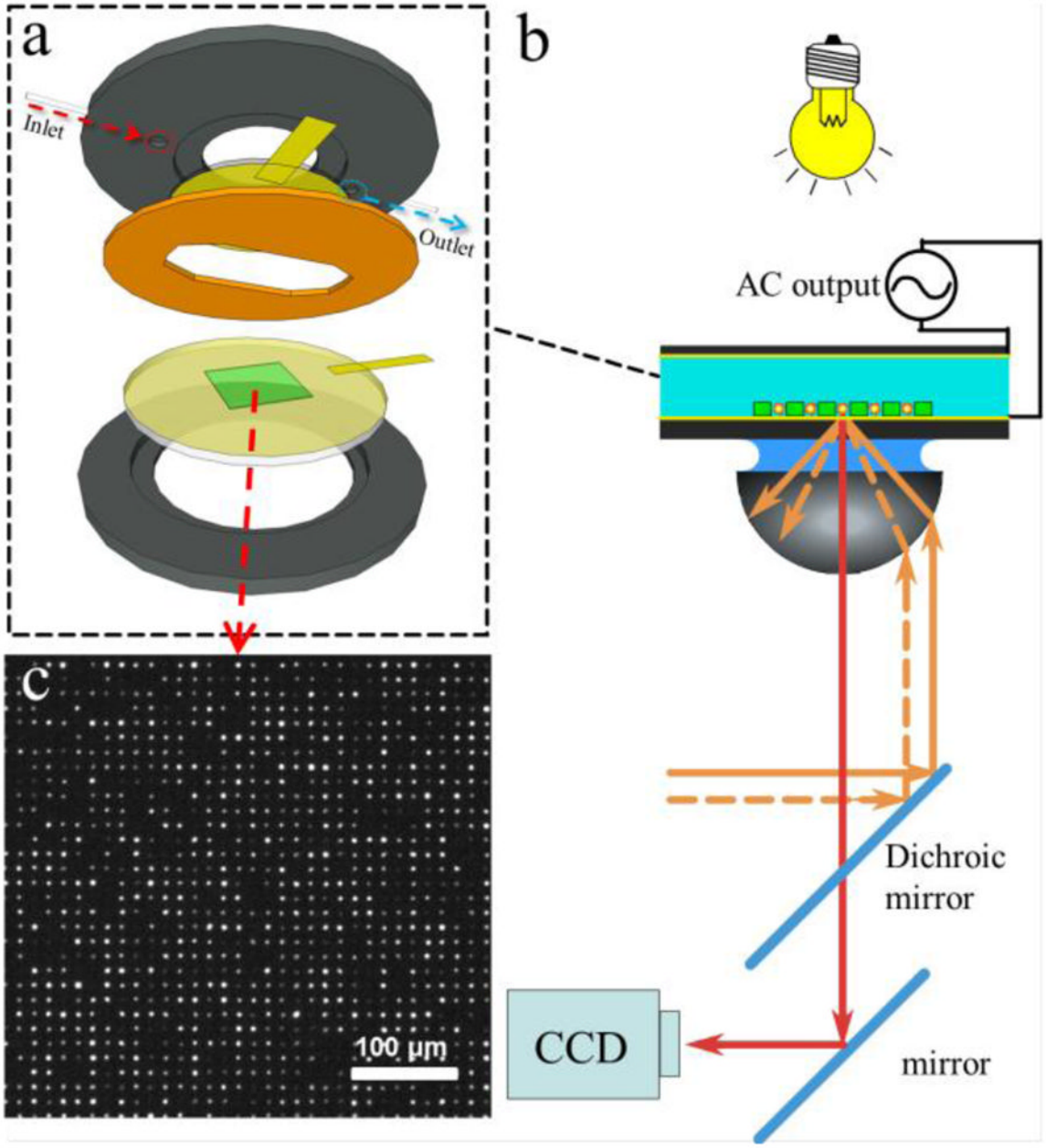

Figure 3.
(a) DEP cell assembly and (b) setup in an optical microscope. The microwell pattern (green) is fabricated on top of the Au-coated glass cover slip (yellow). A sample is sealed with an elastomeric gasket (orange) against Au-coated electrode (yellow) and both are connected to a function generator via copper foil (rectangular yellow pieces). (b) The illumination in transmission mode helped to identify the edges of the microwells. CCD camera captures fluorescent images of the probes from a commercial TIRF setup integrated with a 638 nm laser. (c) Microscope image (10×) of the fluorescent probes assembled inside the microwells.

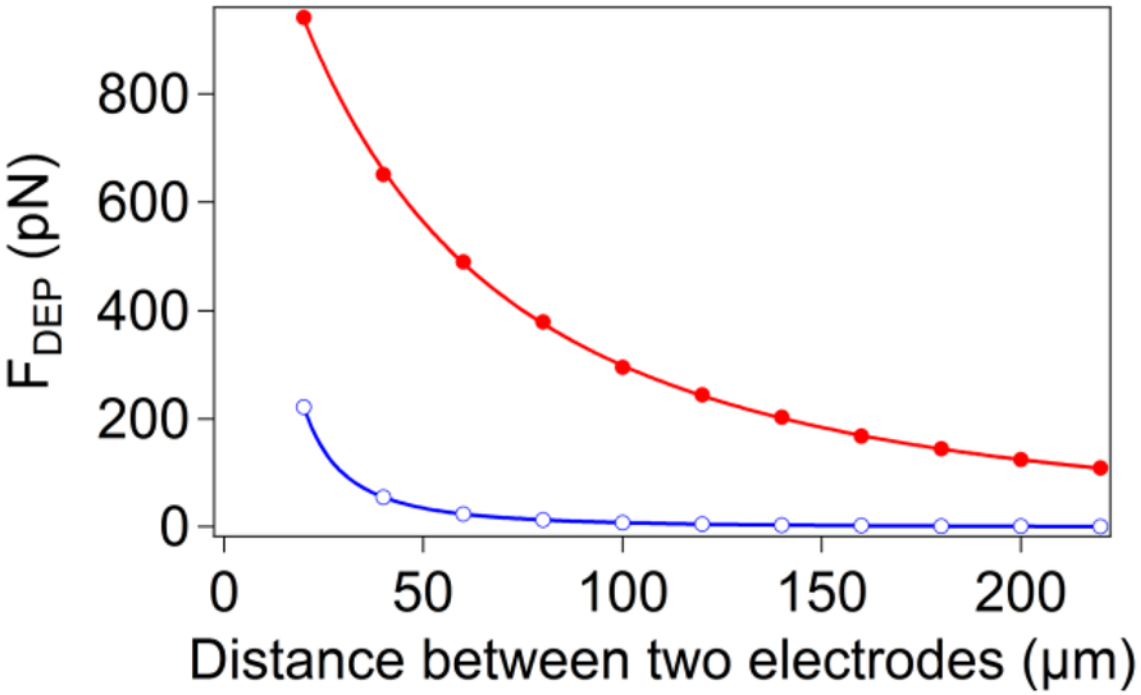

Figure 4.

Simulation results of DEP force as a function of the electrode separation for probes placed 50 nm above the surface of a flat substrate (○), Geometry A, or the bottom of the microwell (●), Geometry C. The parameters used for the simulation were 10 V peak-to-peak voltage with a 3 μm diameter probe. The curves represent the power law $F_{DEP} \propto 1/s^n$ for a Geometry A, where $n=1.987\pm0.001$, and the square of a function in Eq. 6 for a Geometry B.

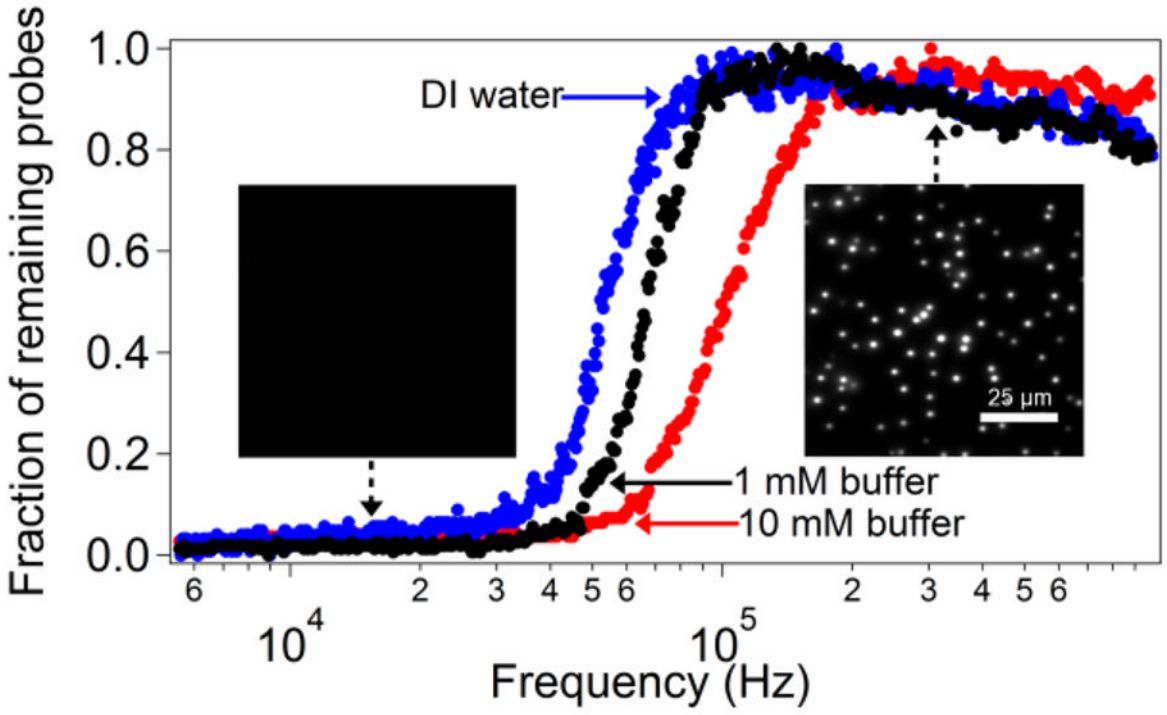

Figure 5.

The number of polystyrene microspheres remaining on the surface of the electrode as the frequency of the applied AC field is changed from 1 MHz to 1 kHz in DI water or phosphate buffer. The number of probes is normalized to the maximum detected during a given sweep. In the negative DEP regime (high frequency), the number of probes slowly increases in the course of the experiment as more probes approach the surface from the bulk of the solution and accumulate at the surface due to attractive DEP forces. (left inset) TIRF image of a sample of probes when 10 V potential is applied at 200 kHz. The probes overcome the electrical double layer repulsion and land on the surface when the field is turned on. The intensity is high, indicating a close proximity to the surface. (right inset) Image of the same sample at a frequency of 10 kHz (10 V potential). Probes are no longer visible using TIRF microscopy.

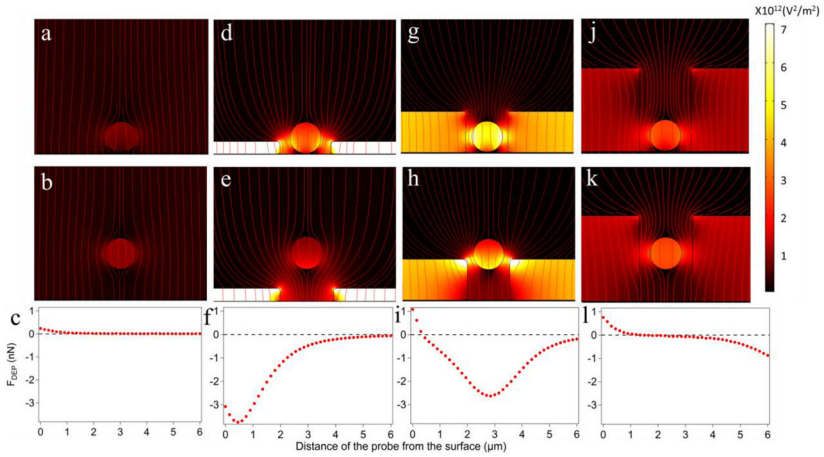

Figure 6.

Electric field distributions in Geometry A (a–c), Geometry B (d–f), and Geometry C (g–l) for a 3 μm diameter probe at 50 nm (a, d, g, and j) and 3 μm (b, e, h, and k) above the surface of the electrode. When close to the surface, the probe is pulled up ($F_{DEP}>0$) by the positive DEP force in (a), (g), and (j), and by the negative DEP in (d). The red streamlines represent the electric field. The surface plots are $\boldsymbol{E}^2$ and all six graphs share the same scale. (c), (f), (i), and (l) The DEP forces versus distance from the surface when the 3 μm probe is moving away from the electrode.

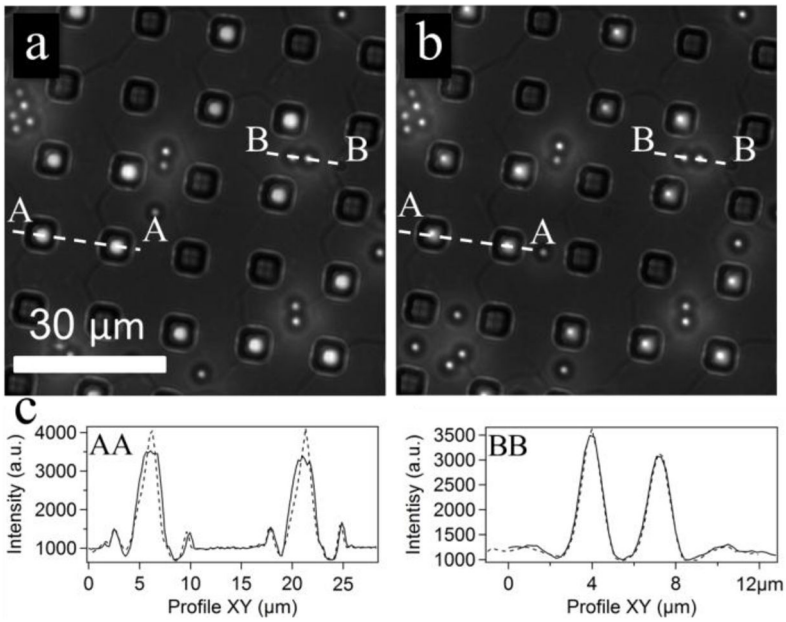

Figure 7.

Epi-fluorescence images of the probes assembled in wells with Geometry C. (a) The probes are pushed toward the surface by a negative DEP force at high frequency (100 kHz) and (b) levitated above the surface by a positive DEP force at low frequency (1 kHz) (V_{pp}=10 V). The probes go slightly out of focus as indicated by their intensity profiles (c) when the frequency is switched from high (a) to low (b). Small bright spots are beads settled on top of the SU-8 surface between wells. Their positions do not change (c). The solid lines in (c) represent the profiles for 100 kHz AC field, while the dashed lines correspond to 1 KHz.

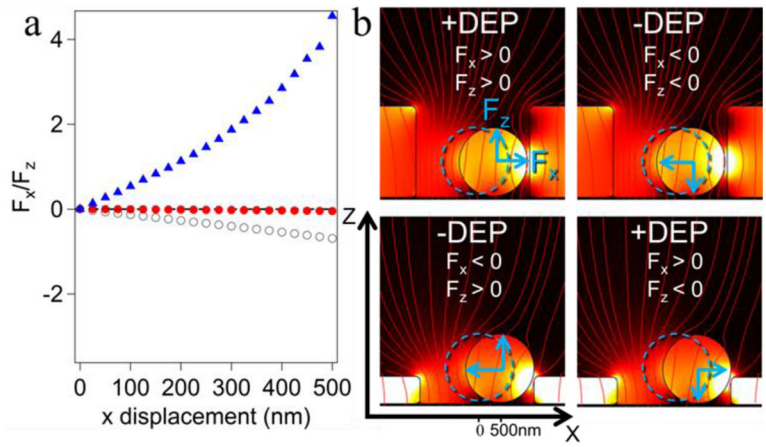

Figure 8.

(a) The ratio of lateral forces to normal forces as functions of lateral displacement of the probes from the well axis for microwell DEP cell with Geometry B (Figure 2b,▲), Geometry C (Figure 2c, ○), and Geometry D (Figure 2d, ●). (b) Blue dashed outlines show the centered position of the probes and the blue arrows show the direction of the normal and lateral forces acting on the probe in each situation (positive or negative DEP). These forces were calculated using a 2D well to reduce calculation time.

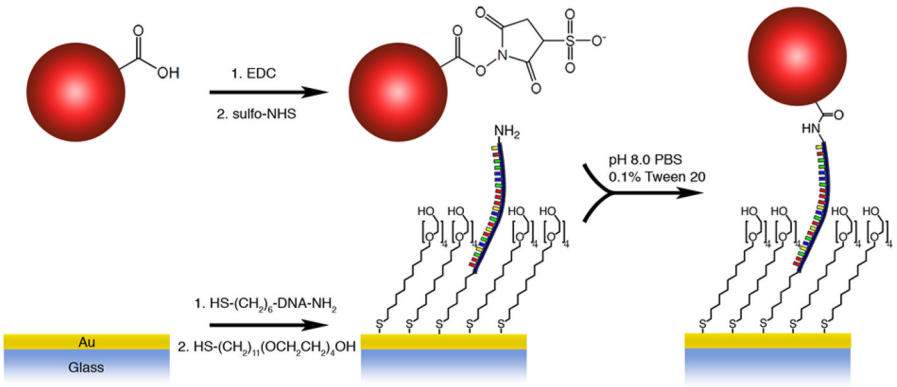

Figure 9.
Reaction scheme of the probe and ssDNA attachment to gold electrode.

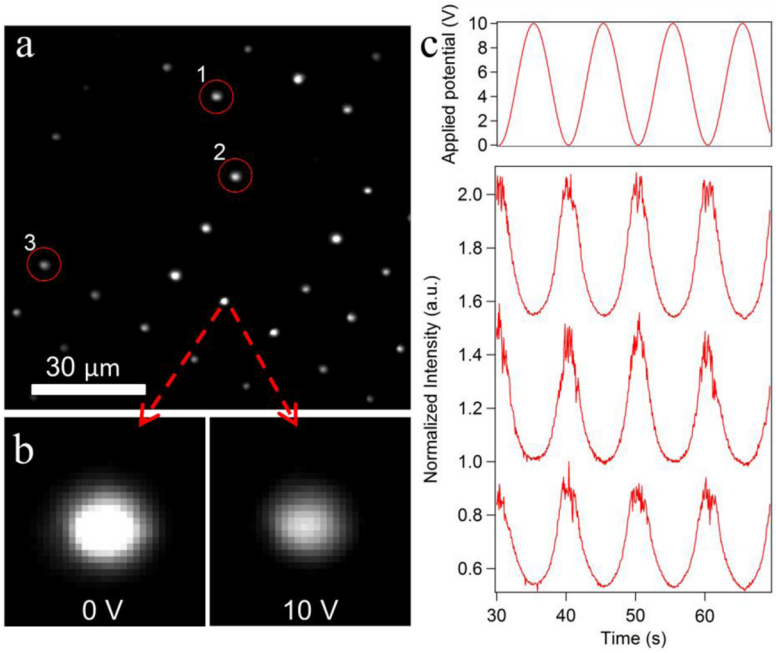

Figure 10.

(a) TIRF image extracted from a movie of the beads bound to ssDNA molecules attached at low density at the bottom of the well s. The image was taken at 0V (i.e. when the probes were closest to the surface). (b) When the AC voltage amplitude changes from 0 V to 10 V, the brightness of the probe drops approximately 50%, consistent with the probe being pulled away from the surface and the DNA molecule being stretched. (c) Applied potential and raw fluorescence intensity data (normalized to a maximum intensity observed in a given trace) versus time for three beads circled in part (a). Intensity traces are shifted with respect to each other for clarity.